AIAA AVIATION Forum
13-17 June 2016, Washington, D.C.
46th AIAA Fluid Dynamics Conference

10.2514/6.2016-3254

Influence of Vortical Interactions on Thunniform Fish Motions

Kislaya Srivastava*and Karthik Duraisamy†
University of Michigan, Ann Arbor, Michigan 48109

Fish-like body motions are modeled and the impact of vortices generated by the motion is analyzed. Specifically, numerical investigations of self-propelled swims of thunniform fish are performed in a low Reynolds number, viscous and nearly-incompressible regime of flow. By computing the flow around a deforming fish-like body, the formation and accumulation of large vortex structures at the anterior and their effect on the overall motion is investigated in detail. Large vortical structures which detach from the anterior and travel downstream are found to affect the self-propulsive motion of the fish either constructively or destructively. The interaction of these vortical structures with the fish-body and tail wake is studied in detail. The deformations of the spine and swim modes are improved in efforts to minimize/eliminate anterior vortex accumulation with the goal of providing stable swims for motions with high tail-tip amplitudes.

I. Introduction

THE modeling and simulation of fish locomotion is of interest in both life sciences and engineering applications. It has the potential to provide explanations to unanswered questions of biological evolution and aquatic physiology of marine animals. This could, in turn, enable us to develop optimized hydrodynamic designs of under-water devices that adopt self-propulsion to achieve extraordinary propulsion efficiencies, acceleration and maneuverability while functioning in non-uniform inflow conditions. Several experimental[1–6] and numerical investigations[7–12] have identified morphological and kinematic attributes that lead to a diverse set of propulsive mechanisms. Self-propulsion using undulations of the body and caudal fins (BCF) involves the traversal of a propulsive wave along the fish body in a direction opposite to the overall motion and a speed greater than its swimming speed. Two main swimming mechanisms that have been identified[13–15] are due to the added-mass and vorticity (i.e. lift-based).

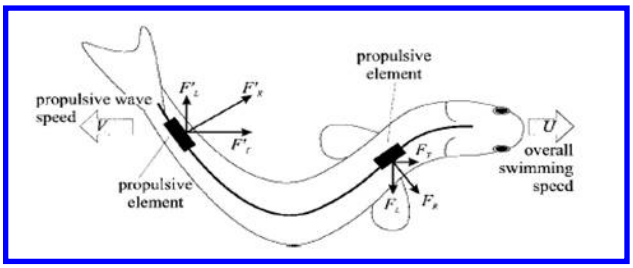

Figure 1. *Thrust generation due to added-mass in BCF propulsion. Combined thrust from all the propulsive elements propels the fish. Magnitude of the thrust contributed by each element increases toward the tail.*[13,14]

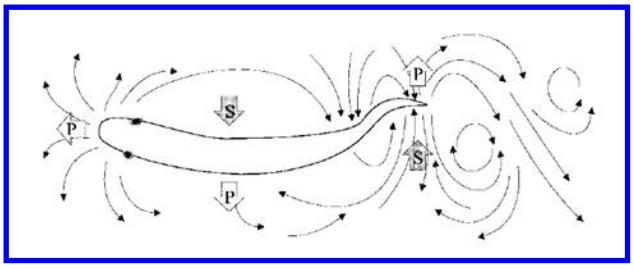

Figure 2. *The flow field around the body of a carangiform swimmer, as obtained from PIV data. The symbols P and S correspond to pressure and suction zones that form the basis of the undulating pump mechanism.*[14,15]

In the added-mass description,[13] shown in Figure 1, the force exerted by the medium on each small segment of the fish body is a reaction to the force generated to increase the momentum of the water being pushed backwards. This reaction force being normal to the body segment, comprises of a thrust component

*Master of Science in Engineering, Department of Mechanical Engineering.
†Assistant Professor, Department of Aerospace Engineering, AIAA Member.

in the direction of overall motion that contributes to forward propulsion, and a lateral component that sheds water laterally and leads to significant losses, introducing tendencies for the anterior part of the body to sideslip and yaw. The tail acts as the primary thruster where the thrust component is larger due to higher amplitudes and speeds that accelerates the water more.

Vorticity mechanisms are demonstrated by Muller et al.[15] with an "undulating pump" mechanism, shown in Figure 2, wherein pressure and suction zones appearing in the flow pattern create a circulating flow around inflection points of the body. This circulating flow propagates along the body, and reaches the caudal fin and interacts with the bound vortices generated by tail movements, combining into discrete vortices shed in the wake. Particle image velocimetry data concluded that a third of the energy being shed to the water is provided by the anterior body. The remainder is generated by the tail. Rosen[16] conducted flow visualization experiments of Carangiform motions, and observed vortices that were being generated by the anterior half of the fish body and thus, proposed a "vortex peg" mechanism wherein the fish thrusts its body against these structures. The rotational energy in the vortical structures is exploited to move forward. Recent visualization experiments,[17] however, observe no such fully formed attached vortices, rather providing evidence for suction and pressure zones in the flow pattern.

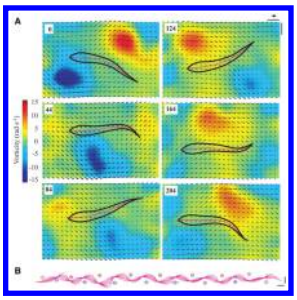

Figure 3. Interaction of trout with cylinder vortices.[18] *(A) Time series (ms) of body outlines (black) and mid-lines (purple) superimposed onto vorticity and velocity vector plots of the cylinder wake. Arrows indicate flow direction and magnitude. Red and blue represent clockwise and counterclockwise vorticity (radians per second), respectively. (B) Mid-lines for seven consecutive tail-beats, beginning from right to left, of which (A) is a subset. The trout carefully maneuvers around the vortex structures, extracting their rotational energy and improving propulsion.*

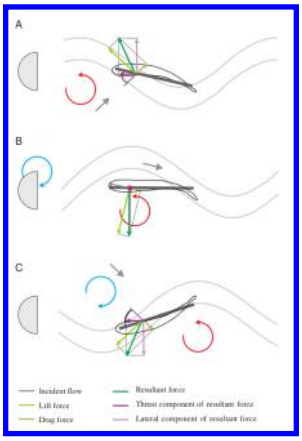

Figure 4. Schematic of the hypothesized hydrodynamic mechanism of the Kàrmàn gait.[19] *A low-pressure, counter-clockwise vortex (red circle) is shed from the cylinder and approaches the head of the trout (A), causing the incident flow (gray arrow) to be directed at an angle to the body (simplified as the wide, dark gray line). The region of reduced flow behind the cylinder is illustrated by the sinusoidal light gray lines. The relatively large angle of attack of the body produces a lift force (light green arrow) normal to the path of the incident flow and a drag force (olive arrow) parallel to the flow. The resultant force (green arrow) can be decomposed into a forward component (purple arrow) and a lateral component (lavender arrow). At a small angle of attack (B), such as when a vortex is directly to the side of the body, the lift force causes the fish to only move laterally, since the thrust component of the lift force is zero (purple dot). A clockwise vortex (blue circle) is forming on the opposite side of the cylinder. The shed clockwise vortex is now just upstream of the trout in (C), and the counterclockwise vortex has drifted past the body of the trout. Force vectors are similar to that in A, only opposite in direction. Due to vorticity decay, the upstream vortex has a lower pressure than the downstream vortex, which may facilitate station holding.*

Fishes are well-known to commonly reside in high energy environments, preferring to associate with turbulent flows generated from water flowing past inanimate objects.[20,21] They have been observed to constructively utilize the energy in the inflow which results in significant improvements in locomotive efficiency[14,18,19] see Figures 3 and 4. This is achieved through properly adapting their BCF motions to incoming vortical structures. Gopalakrishnan et al.,[22] conducted experimental studies on a foil that was provided with a heave and pitch motion while placed in an incoming vortex street generated by a cylinder source. Their experiments found the propulsive efficiency and wake vorticity patterns to be sensitive to the phase between the oncoming vortices and foil motion. Numerical and theoretical analyses presented by Streitlien et al.[23] found that the propulsive efficiency exceeds 100% when the foil motions correspond to an order of half of the vortex street width and the vortex street is above a certain strength. They state that the timing, or phase, of the foil motion has to be such that it is brought in close contact with individual vortices in the inflow. These evaluations showcased the demonstrated ability of energy extraction from incoming vortices by fishes since their shapes are comparable to airfoils. Effective interception of oncoming vortices with optimized angle of attacks would enable increased thrust through addition of vortex rotation. They also demonstrate sensitivity of fish swims and propulsive thrusts to incoming vortex structures. A need arises for proper control of body motions so as to obtain optimized and favourable vortex interactions.

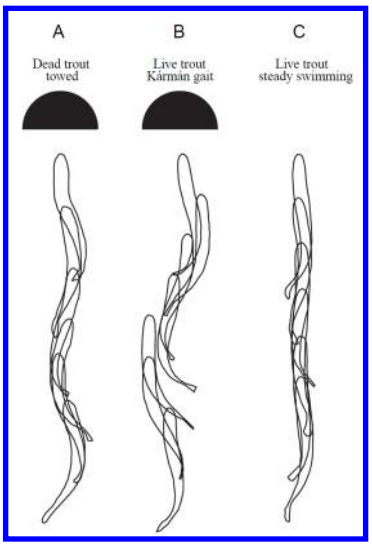

Figure 5. *Body outlines of a dead trout towed behind the cylinder[24] (A), a live trout Kàrmàn gaiting behind the cylinder (B) and a live trout swimming in uniform flow (C). Body outlines have been displaced upstream at evenly spaced intervals to facilitate visualization of kinematics. Similar to a live trout Kàrmàn gaiting, a dead trout towed in the wake of a cylinder oscillates laterally with high amplitude and has a tail-beat frequency similar to the expected vortex shedding frequency. The body wavelength is also longer than the expected wake wavelength, confirming that live fish can synchronize to the vortex street in a largely passive manner. Dead and live trout behind the cylinder adopt the same mean head angle. However, live trout head angles have a wider range of values and a higher variance, indicating a larger change in head angle during the Kàrmàn gait compared with dead trout.*

These experiments serve to explain the "Gray's Paradox"[25] which states that power required for cruising of dolphins exceeded their muscle power output by a factor of 7. Making adjustments and corrections to Gray's estimations, the new hypothesis seems to be supported by the flow visualization experiments of swimming fish[26] and robots,[27] as well as the experimental and simulation results obtained from oscillating foils that extracted energy from incoming vortices.[22,23,26] Based on the exploration of the effects of oncoming vorticity on foil performance, basic modes of foil-vortex interaction have been defined as follows:[28]

- Vortex interception mode: wherein the leading edge of foil intercepts the incoming vortices, thrust increases and wake downstream of the foil is substantially altered through strong foil-vortex and incoming cylinder-vortex interactions.
- *Slaloming mode:* wherein the leading edge of foil approaches but does not intercept the oncoming vortices. The wake consists of pair of vortices, one produced by the foil and one by cylinder. This mode is found to result in high propulsive efficiency.

Liao[24] utilized electromyography to investigate trout muscle activity during Kàrmàn gait, in order to test three hypotheses: 1) Rhythmic axial muscle activity pattern in Kàrmàn gaiting fish differs from the rostro-caudal travelling wave of muscle activity typical of fishes swimming in uniform flow; 2) Cylinder vortices rather than axial muscle activity dominate Kàrmàn gait kinematics; 3) Short bouts of Kàrmàn gaiting can proceed at times without any muscle activity. The experiments concluded that while the entire body was participating in a large-amplitude mechanical wave, only the anterior muscles were being selectively activated to exploit incoming vortices. This was different for the case of freely behaving fishes which show sequential anterior-posterior wave of axial muscle activity that drives the undulatory motion in uniform flows, which was being abandoned during Kàrmàn gait. The muscle activity however was not correlated to the head amplitude during Kàrmàn gait, which indicate that anterior muscles are utilized in order to maintain proper body posture for stability and control, and that the overall head motion is determined by oncoming vortices. Advancing regions of low pressure down the body cause the fish to adopt a travelling waveform motion. Importance of incoming vortices on Kàrmàn gait kinematics were further demonstrated on a dead trout, wherein passive thrust generation was observed after body kinematics synchronized to the Kàrmàn street.

Motivated by these experimental and numerical studies, we intend to investigate the effect of vortex structures formed by the anterior part of the fish on the overall fish motion. These structures might have a significant impact on the self-propulsion velocity of the fish, either constructively or destructively. Since these vortex structures detach from the nose and travel closely along the fish-body length, it becomes possible to extract their energy and augment propulsion by controlled/adapted oscillations of the fish body, thereby regaining energy lost, increasing propulsion efficiencies and motion stability. The studies are carried out in two dimensions, even though the experimental results mentioned above related to three-dimensional flows in the turbulent regimes. Three-dimensional wakes are found to show distinctive features that can affect fish locomotion even at low Reynolds numbers.

The purpose of this study is to adapt an efficient simulation technique to the study of body self-propulsion in efforts to investigate the nature of interactions with vortex structures with the fish-body and tail wake, which can either improve or adversely affect fish motion, and make attempts to improve propulsion by altering spine deformation, comparing results obtained with studies mentioned above.

II. Parametric modeling of the Thunniform fish body

A. Modeling of Steady Shape

In this work, the self-propelling fish body is modelled as a deformable airfoil. Periodic deformations are then imposed on the airfoil steady shape assuming no external forces are required for it. Here, we assume the fish density to be constant and equal to the fluid density.

Fish swimming can be classified into two major categories:[29] Body/Caudal fin (BCF) propulsion or Median/Paired fin Propulsion. There are five BCF groups that differ in the fraction of their body that is displaced laterally, namely: Anguilliform, Sub-carangiform, Carangiform, Thunniform, and Ostraciiform. BCF motions can in turn be periodic or transient. Here, only the Thunniform periodic BCF movements with the absence of a caudal fin were investigated.

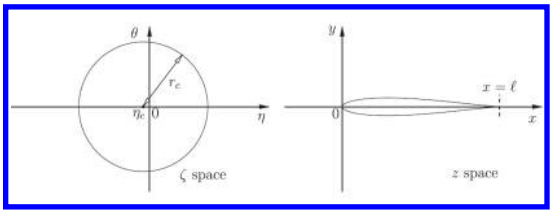

Figure 6. *Sketch of the steady shaped fish profile obtained from Kàrmàn-Trefftz transform*[7]

The steady shape is described as in Reference 7 by the Kàrmàn-Trefftz conformal transformation, rather than a simple Joukowsky transformation, to achieve realistic and comparable profiles. A circle in the ζ-complex plane with center (η_c,θ_c) is transformed into the z-plane using (see Figure 6) :

$$z = n\frac{\left(1+\frac{1}{\zeta}\right)^n + \left(1-\frac{1}{\zeta}\right)^n}{\left(1+\frac{1}{\zeta}\right)^n - \left(1-\frac{1}{\zeta}\right)^n} \tag{1}$$

where the trailing edge angle is α = *(2-n)*π. The steady state fish shape is defined by four shape parameters: η_c , θ_c , α and L, L being the length of the fish. For symmetry, $\theta_c = 0$. η_c , α, L can be parameterized to obtain various BCF fish profiles. For our Thunniform case, thickness is defined by η_c = -0.04, and the trailing edge by $\alpha = 5°$. The steady shape is translated and scaled so as to place the nose at origin and set $L = 1$.

B. Modeling unsteady motion

The body shape in unsteady motion is prescribed using the periodic swimming law.[7] The fish spine, given by $0 \le x \le 1, y = 0$ is deformed to fit a curve $y(x,t)$ keeping the spine length as unity throughout. This imposed periodic motion is given by:

$$y(x,t) = a(x)sin(2\pi(x/\lambda + ft)) \tag{2}$$

where the curve amplitude is defined by : $a(x) = c_1x + c_2x^2$. Since the nose of the fish is placed at origin, the wavy motion is centered on the nose. Defining s as the curvilinear coordinate of the deformed backbone $0 \le s \le 1$ and fixing *s=0* at *x=0*, for a given coordinate s, the abscissa *x(s)* is found by inverting:

$$s = \int_0^1 \sqrt{1 + \left(\frac{\partial y(x',t)^2}{\partial x'}\right)}\, dx' \tag{3}$$

The corresponding $y(s) = y(x(s),t)$ can then be calculated. The corresponding deformed fish body profile is generated with the assumption that the profile points remain normal to the spine during deformation as shown in Figure 7.

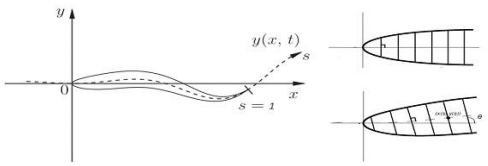

Figure 7. *Swimming shape*[7] *with periodic deformation. Points on profile remain normal to the spine.*

Swimming Parameters λ , f, c_1 and c_2 are given values of 1.25, 2 , 0.1 and 0.9, respectively, to represent limited oscillations of Thunniform modes and a maximum tail displacement of $A = 0.2$ is imposed by scaling the amplitude parameters.

The fish is assumed to start from a state of complete rest. As the flow solutions are obtained, the displacements of the fish body are updated by integrating the two-dimensional equations of motions using Euler explicit time-stepping.

III. Numerical discretization

To accurately resolve the flow, a good quality mesh with appropriate resolution needs to be generated. We utilize an overset mesh system to adapt to the dynamically deforming fish profile. Due to the largely time dependent deforming nature of the fish profile, the choice of a single mesh system would be inefficient. Instead, an overset mesh system is considered, which has a refined fish body mesh resolving the near field overset inside a coarser background mesh resolving the far field. This efficient meshing strategy requires mesh generation of only the fish body every time step while using the same background mesh for all the time steps.

Overset meshing involves the construction of a grid system made up of blocks of overlapping structured grids. The connectivity across grids is established using implicit hole cutting strategy[30] which automatically determines the connectivity in a given set of mesh systems. This has the advantage that different grids can be generated independent of each other and can be placed in the region of interest without any distortion. Such flexibility is invaluable in our problem since meshes move relative to each other. The additional work required in identifying points of overlap between meshes and interpolation of the solution in this overlap region, and possibilities of a loss of the conservation property of the numerical scheme can be minimized by proper selection of mesh structure and placement. The background grid is a Cartesian mesh of size 205×181 with the outer boundaries 10 body lengths away on the front, top and bottom, and 20 body lengths away on the aft of fish, see Figure 8(a). The body mesh uses (Figure 8(b)) a C mesh of size 241×31 in the wrap-around and normal directions, respectively, (outer boundary at $\tilde{0}.17$ fish lengths), and is re-generated at the beginning of each time step.

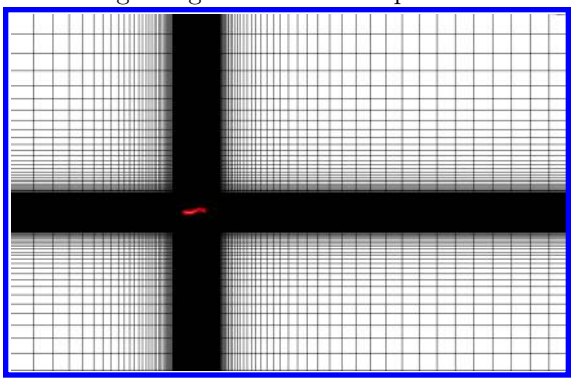

(a) *Fish-profile mesh (red) overset on a single, background mesh (black)*

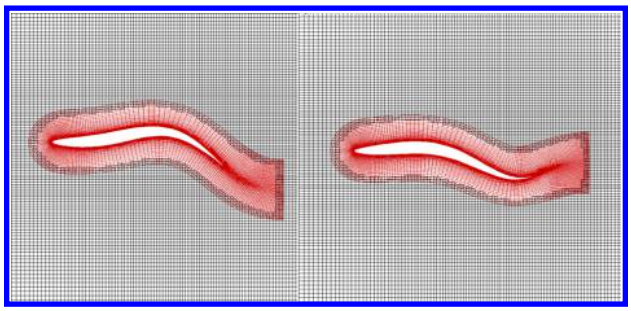

(b) *Fish-profile mesh (red) being generated every time step for one oscillation and reused periodically*

Figure 8. Overset mesh system for the flow domain

Care is taken to avoid cross-over of the fish-profile grid cells when the fish profile deforms and it is ensured that the mesh cells of the background mesh are comparable to those around the boundary of the fish-profile mesh for accurate interpolations. After successfully generating suitable mesh system, next the flow solutions are computed.

The numerical simulations are carried out using OVERTURNS[30–34] solver, which computes solutions to the compressible Navier–Stokes equations. A fifth-order accurate upwind scheme is used to compute the inviscid fluxes, while the viscous terms are discretized using fourth-order accurate central differencing. The maximum Mach number encountered in the simulations is 0.1, thus compressibility effects are negligible. Low Mach number preconditioning is used to accelerate convergence. Implicit time integration is used with dual-time stepping. The flow is modeled to be viscous and laminar, with a nominal chord-based Reynolds number of 1000. In non-dimensional coordinates, the length of the fish is unity and the viscosity is set to

0.0001.

IV. Exploration of the flow

Starting from a state of rest, we provide a tail tip amplitude of 0.2 for our fish. A self-propulsive 2D swim is obtained in a viscous, laminar flow with a maximum chord-based Reynolds number of 1000. Results are as follows:

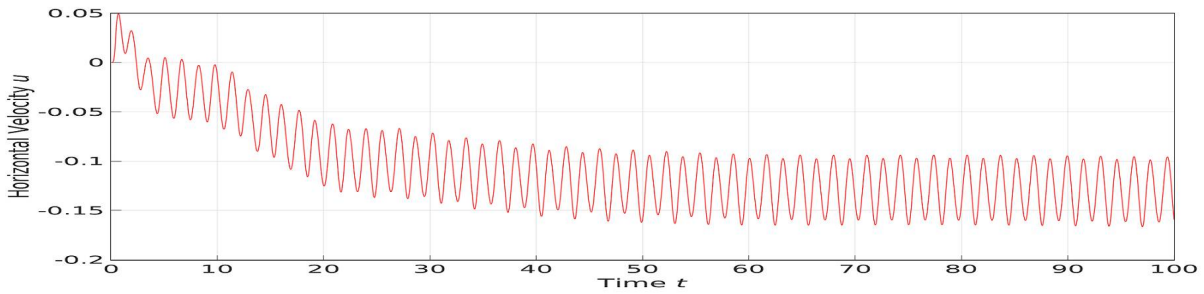

Figure 9. Horizontal velocity u vs time t. *Starting from rest, the thunniform fish proceeds towards a steady velocity, oscillating around -0.1292.*

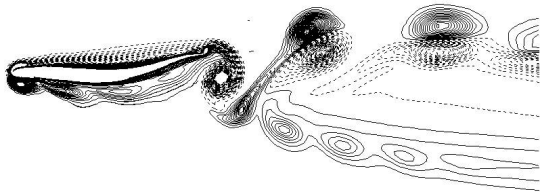

Figure 10. *Vorticity representation of the wakes generated by Thunniform swimming movements at $Re = 10^3$ and $A = 0.2$. Figure is plotted for $-10 \leq \omega \leq 10$*

Figure 11. *Results obtained by Bergman and Iollo[7] for Thunniform swimming movements at $Re = 10^3$ and $A = 0.4$. Figure was plotted for $-100 \leq \omega \leq 100$*

The fish is found to move forward (Figure 9; displacement in the -x direction) after accelerating towards a steady state velocity from rest. The average horizontal velocity $|\bar{u}|$ of the fish from time $t = 0$ is found to be -0.1001 with a maximum velocity reaching $|u_{max}|$ = -0.1594. After the swim is fairly steady ($t > 60$), the average velocity of the fish attains a value of -0.1292. At this stage, the velocity and force coefficients appear to have steady-periodic oscillations around their mean value. It is to be noted that the fish also has a small vertical velocity, that propels it in the positive y direction.

The wake vortex structures (Figure 10) are qualitatively compared to those obtained by Bergman and Iollo[7] (Figure 11) for thunniform profiles at Re=1000. Our wake structures are found to be a distorted compared to Bergman and Iollo. It is to be noted that, unlike their model, no transition function is used to ensure zero lift at the start of the motion to enable strict horizontal fish motion. Thus, in this work the fish has a net vertical velocity and hence vertical displacement. This could explain the differences in wake structures. Another difference from their model is a lower magnitude for tail tip displacement. This results in lower velocities for fish in this work. For our fish, small vortical structures were found to be accumulating

at the nose of the fish, which detached at random instances and travelled along the fish body, interacting with the tail wake. This is not observed by Bergmann. Higher swim speeds of their fish could be a possible explanation to lack of vortices being accumulated at the nose. Higher swim speeds would imply eradication of vortex structures/accumulation at the nose.

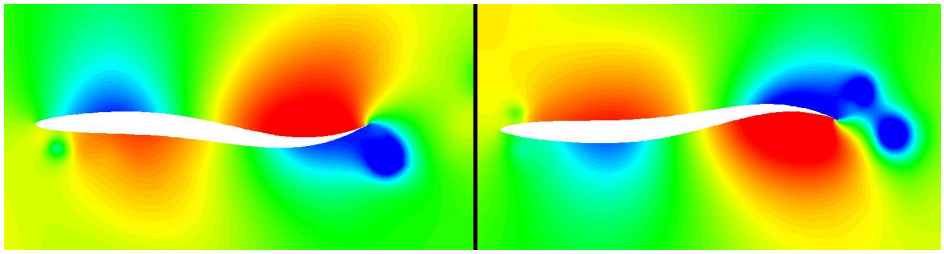

Figure 12. Pressure plots at different time instances. *Pressure plots seem to be in accordance with Muller's[15] undulating mechanism consisting of regions of high(red) and low(blue) pressure travelling along the body*

The pressure plots yield a good level of similarity with Muller's[15] undulating pump mechanism and visualization experiments[17] wherein regions of pressure and suctions are formed due to the oscillating motions of the fish body. Shown in Figure 12, these create regions of circulating flow (confirmed by vorticity plots) which travel along the body surface. Reaching the tip of the tail, they interact with vortex structures formed by tail-tip motion. It is uncertain whether this is the mechanism for formation of discrete vortex structures in the wake. These pressure patterns appear to be periodic after the fish attains steady velocities.

Small vortex structures are noticable and are created at the nose (anterior) of the fish body, in accordance with observations of Rosen.[16] While these structures might persist for a certain amount of time, they eventually travel along the fish body and combine with the wake generated by the fish tail. While most of these structures are extremely small in comparison with those generated at the tail wake, possibility exists of fairly large vortex structures accumulating around the nose, which detach and travel along the fish body affecting its motion significantly. These instances are noticed in swims with higher tail-tip amplitudes and higher Reynolds number. Vortex interactions at higher Reynolds numbers for $A = 0.2$ are explored below.

A. Constructive vortex interactions

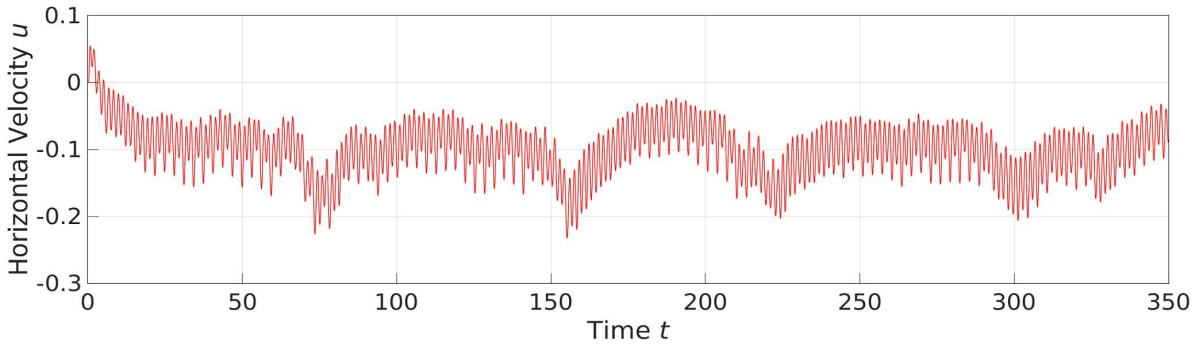

Figure 13. Horizontal velocity u vs time t. *Starting from rest, the thunniform fish proceeds towards a steady velocity, oscillating around -0.1. Sharp increases in velocity magnitude can be observed in the plot at random instances for a short amount of time, implying a sudden acceleration due to reduction in drag forces.*

The simulations were carried out until the fish travels 50 times its body length to obtain a large time span in which different vortex-body interactions could be observed and studied. The average horizontal velocity $|\bar{u}|$ of the fish from time $t = 0$ is found to be 0.09924 with a maximum velocity reaching $|u_{max}| = 0.2323$. The velocity and force coefficients that appeared to have steady-periodic oscillations around their mean value in the previous case, are now affected by fairly large vortex structures that detached from the nose and traveled along the fish profile, visible in Figure 14. This causes random fluctuations in their values during the swim.

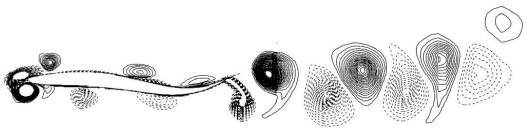

Figure 14. *Vorticity representation of the wakes generated by Thunniform swimming movements at higher Re. Figure is plotted for -10 $\leq \omega \leq$ 10*

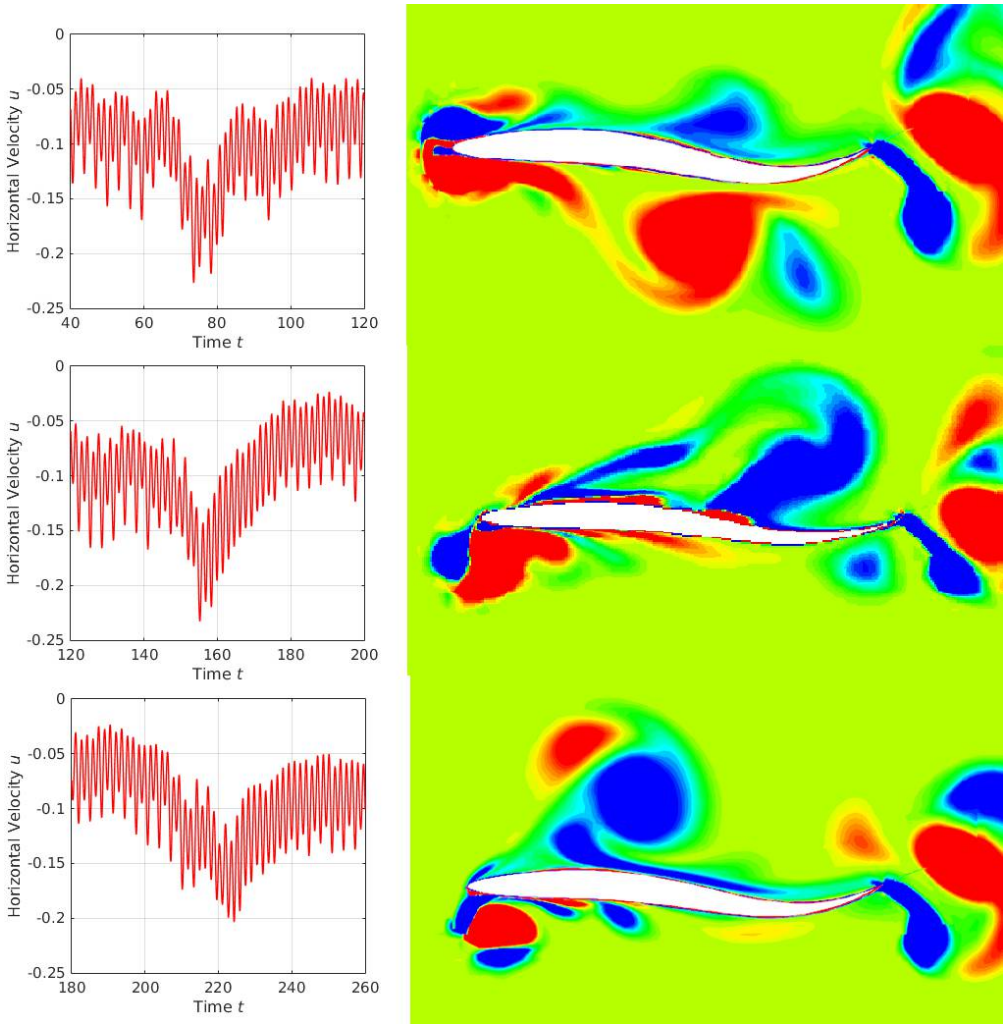

Figure 15. Constructive interaction large vortex structures with the fish body. *Vorticity representations at time instances where sudden spikes in velocity magnitude are noticed. Red (counterclockwise) and blue (clockwise) vortices interact with the body surface as the fish moves forward (-ve x direction). (From top to bottom) Solution frames at t = 75.3, 155.8, 213.5, where the velocity magnitude has an increasing spike, clearly shows large structures travelling along fish body and adding their rotations to fish movement. The velocity increase persists until these structures combine with the tail wake.*

These instances are noticeable in Figure 13. The velocity magnitude is found to deviate significantly from its steady periodic oscillation and increase substantially. This increase only persists for a short amount of time and appears to occur in a fairly random fashion. Visualizing the flow solutions at these time instances, we notice the presence of a fairly large vortex structure, generated at the anterior body, interacting with body surface. The spike in velocity magnitude can be explained by the fish extracting the rotational energy of these vortex structures that reduces the apparent drag and makes it travel faster, in accordance with observed thrust and improvements in locomotion efficiencies through constructive utilization of vortex rotational energies.

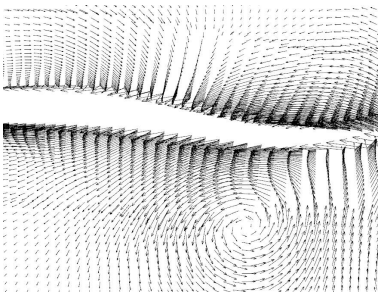

Figure 16. *Vector plot of velocity at t = 75.3 showcasing the addition to rotation from the counterclockwise vortex structure to the forward motion of the fish.*

The vortex interactions for the particular case shown in Figure 15 are constructive, i.e. their rotations add on to the motion of the fish (Figure 16), propelling it faster. These structures, after traversing along the fish body length, join the tail-tip structures in a way that does not disrupt the wake vortices significantly. Thus, the propulsion due to pressure forces as a result of fish body oscillations could be considered fairly stable. Using the same concept, there develops possibilities of vortices with opposite rotations travelling down the fish body length that might decrease propulsion or force movement in the opposite direction altogether. Anterior vortex structures could also significantly disrupt tail wake vortices, resulting in a tremendous drop in pressure-generated self-propulsion. This could cause a stall in the fish motion, wherein the fish would be suspended in its vortices and/or undergo haphazard motions.

B. Destructive vortex interactions

While the above interactions are constructive to the forward motion of the fish, it is also useful to investigate possibilities where anterior vortex generation and consequent body and tail wake interactions could otherwise hinder the motion of the fish (Figure 17). For this motion, the frequency is modified to $f = 1$ in efforts to increase the accumulation of vortices at the nose tip, and maximum tail displacement to $A = 0.4$ to provide the fish with sufficient velocity. The different stages of the fish swim are demonstrated in Figures 18-21.

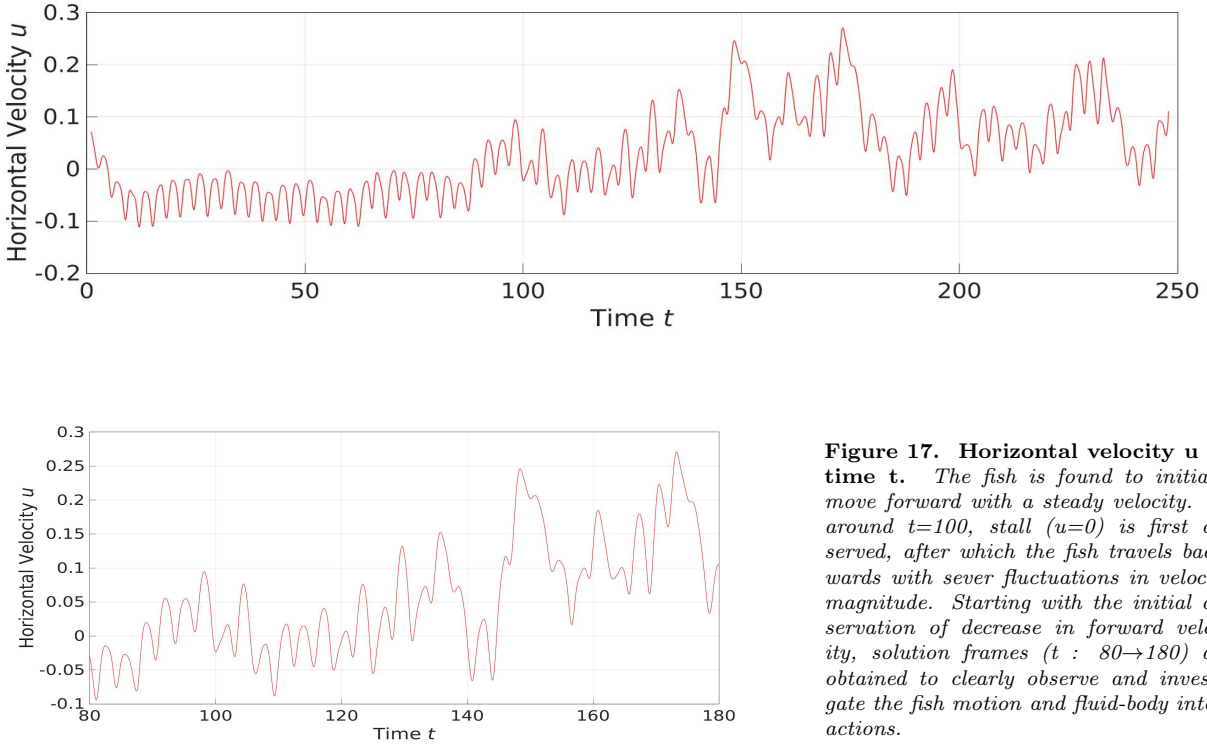

Figure 17. Horizontal velocity u vs time t. *The fish is found to initially move forward with a steady velocity. At around t=100, stall (u=0) is first observed, after which the fish travels backwards with sever fluctuations in velocity magnitude. Starting with the initial observation of decrease in forward velocity, solution frames (t : 80→180) are obtained to clearly observe and investigate the fish motion and fluid-body interactions.*

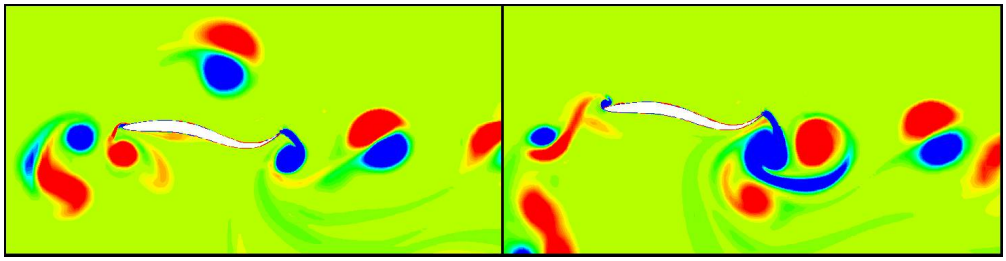

Figure 18. Disruption of tail wake vortices. *(t = 80.6, 94.2) Lower fish velocities and low frequency of oscillations facilitate the accumulation of large vortex structures near the nose of the fish that eventually detach and travel towards the tail wake. The nature of interaction leads to the breaking of the continuous wake vortex street and results in the disruption of pressure-related propulsive forces, slowing the fish motion and causing significant change in drag and lift forces. It is worth noticing in the right frame that the blue (clockwise rotation structure) structure adds opposite motion to the body and also adds to high positive lift.*

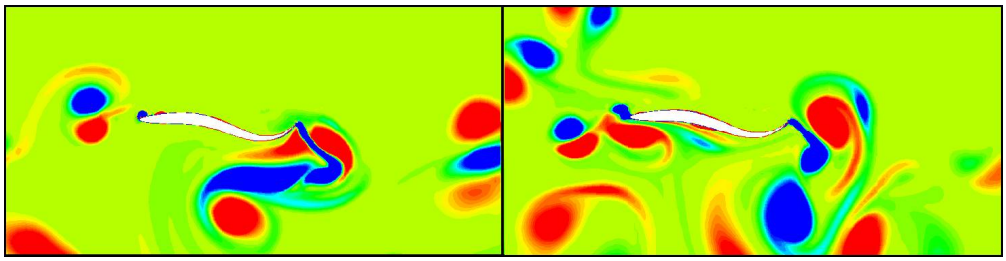

Figure 19. Horizontal translational stall. *(t = 100.5, 113.1) The breaking of the tail vortex street is such that more drag is induced and there is a significant decrease in propulsive forces. This results in the fish slowing down and finally causing its horizontal motion to stall, making it swim in its tail-generated vortices while they accumulate near the tail. Erratic lift forces cause lateral nose movements causing further generation of anterior vortex structures.*

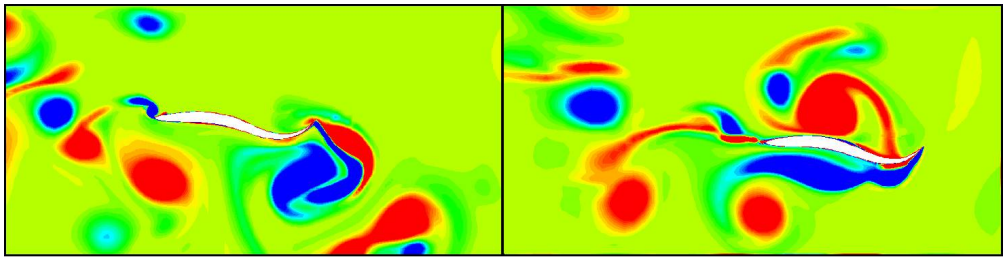

Figure 20. Vorticity induced translation. *(t = 131.9, 150.7) There is a buildup of large vortex structures such that they add their rotation on the body surface in the opposite (+ve x) direction. The fish extracts this energy and proceeds to translate backwards. All the while, these structure persist along the body surface and increase the velocity.*

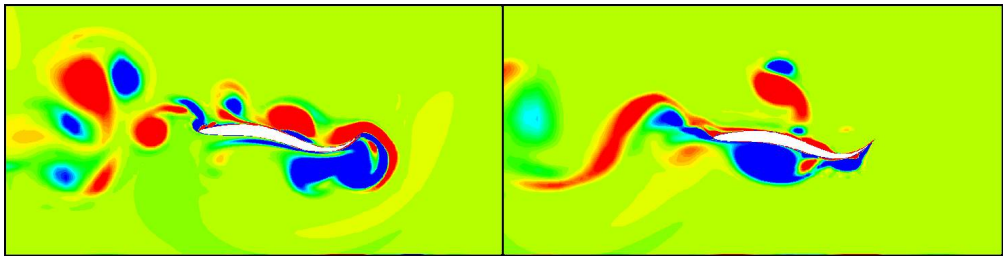

Figure 21. Steady backward translation. *(t = 169.6, 175.9) Vortex structures grow in size due to tail motion and continue to add their energy towards the backward motion of the fish. Fish now gathers momentum in the backward direction and proceeds towards steady motion. It is worth noticing the vortex street from the nose of the fish. The vortices also include extra oscillatory lift forces, which causes the anterior of the fish to undergo lateral oscillations and might lead to increased pressure-related propulsive forces in the opposite direction, complementing the backward motion.*

The propulsion of the fish in a laminar free stream could be attributed to three influential methods: Reaction forces due to added-mass method from the deformation of the fish pushing the water behind, Suction and pressures regions observed that favour motion, and interactions between anterior vortices that add their rotation to fish movement as they travel along the body. We find evidence of vortex interception mode of interactions,[28] after vortices detach from the nose tip, that affect the thrust. Our destructive case experienced substantial alteration of wake structure due to strong anterior-vortex and tail-tip vortex interactions. This was not so in the constructive case. This is in accordance to foil experiments of Gopalkrishnan et al.,[22] where wake patterns were observed to be sensitive to phase between oncoming vortices and foil motion.

From the above studies it becomes clear that anterior vortex structures can play a vital role in the overall motion of the fish. These structures could also severely alter the suction and pressure regions around the fish to either benefit or oppose the stable forward motion of the fish. Altering these regions could in turn favor further accumulation of vortices at the anterior. Thus, these two methods become intertwined. Erratic and opposing movements due to destructive cases could affect direction of reaction forces altogether and the fish might fail to generate substantial forward thrust forces to oppose these unfavourable vortex interactions, causing it to be pulled backwards. It becomes imperative for the fish either to adapt to the generation of constructive vortices so as to increase its propulsion, and/or alter its motion to eliminate destructive interactions to ensure stable forward motion.

V. Exploring the impact of kinematic parameters

Having explored the basic effects of vortical interference on the motion, the following results examine the sensitivity of the kinematic parameters on the propulsive forces.

A. Frequency and Tail tip amplitude effects on fish swim

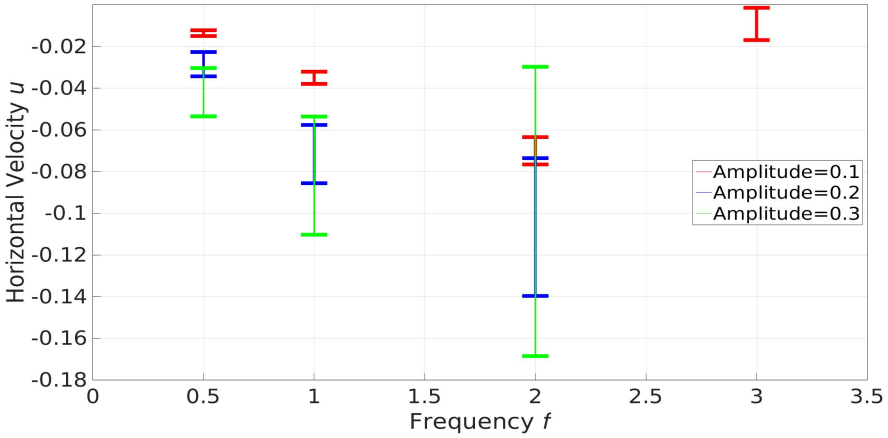

Figure 22. Velocity-vs-Frequency-vs-Amplitude. *Amplitudes 0.1(red), 0.2(blue) and 0.3(green) studied for different frequencies of spine deformations. Larger amplitudes provided with larger values of swim speeds, but also for large variations in velocity limits. Optimum value for frequency was obtained for f =2*

Figure 22 shows the horizontal velocity ranges versus frequency for different values of fish tail tip amplitudes $A = 0.1, 0.2, 0.3$. It can be observed that greater amplitudes provided with swim average and maximum speeds. Higher amplitudes, however, create significant velocity variations and larger velocity ranges resulting in a less smooth motion. Increasing the value for A to 0.4 and beyond, resulted in backward fish swim.

With regards to frequency dependence, we find there exist an optimum frequency $f = 2$, that provides for fastest swim speeds for a given amplitude. As frequency of spine oscillations decrease, the swim slows down. For frequencies greater than 2, only the value of $A = 0.1$ provided for swim motion in the forward direction. Greater amplitudes and frequencies resulted in a backward swim.

For further studies, $f = 2$ will be considered and we sought out to alter fish body deformations to improve/stabilize the swims for higher tail amplitudes.

B. Varying Spine deformations

Our default parametric modeling of the fish body places the fish nose tip at origin. Thus, for our default cases, as well as those by Bergman,[7] the y-amplitude of spine oscillation is zero at the nose, following the periodic swimming law, and increases as we travel along the length of the fish body. Since our simulations provided no corrections for moments, the nose always points towards the −ve x direction. Solutions showcased in section IV have demonstrated that the vortex structures travel along the body and affect the motion of the swim, causing random variations in its velocity, are mostly, if not always, accumulated/generated at/near the nose. These structures, though at times might improve the propulsion of the fish for a short period of time, cause an erratic swim motion. It thus becomes critical to mitigate or control these structures for a stable, steady swim motion. With this in mind, we seek to investigate what happens when the nose tip is provided an oscillating motion, by centering our oscillations at the anterior of the fish body. These anterior oscillations can be modelled to prevent the formation of anterior vortex structures and thus, lead to reduced energy losses and a stable, efficient swim. However, if the generation of these structures is imminent, anterior oscillations can be altered to destroy/disrupt accumulation of large anterior vortex structures, breaking them up into smaller structures that have negligible impact on the motion of the fish as they travel downstream. Possibility exists of this being controlled to favor periodic generation of constructive vortices, from which energy can be extracted steadily. This would lead to improved propulsion efficiencies.

Motion to the head/nose was provided by shifting the value of zero spine deformation into the body (δ from the nose tip along the spine), i.e., our coordinate system origin was placed at spine length δ from the nose tip. Using the periodic swimming law described in Eq.2:

$$y(x,t) = a(x)sin(2\pi(x/\lambda + ft))$$

three kinds of altered spine deformation motions can be provided:

1. Positive Head : wherein if $x < 0, y = y(x,t)$
2. Negative Head : wherein if $x < 0, y = -y(x,t)$
3. Fixed Head : wherein if $x < 0, y = 0$

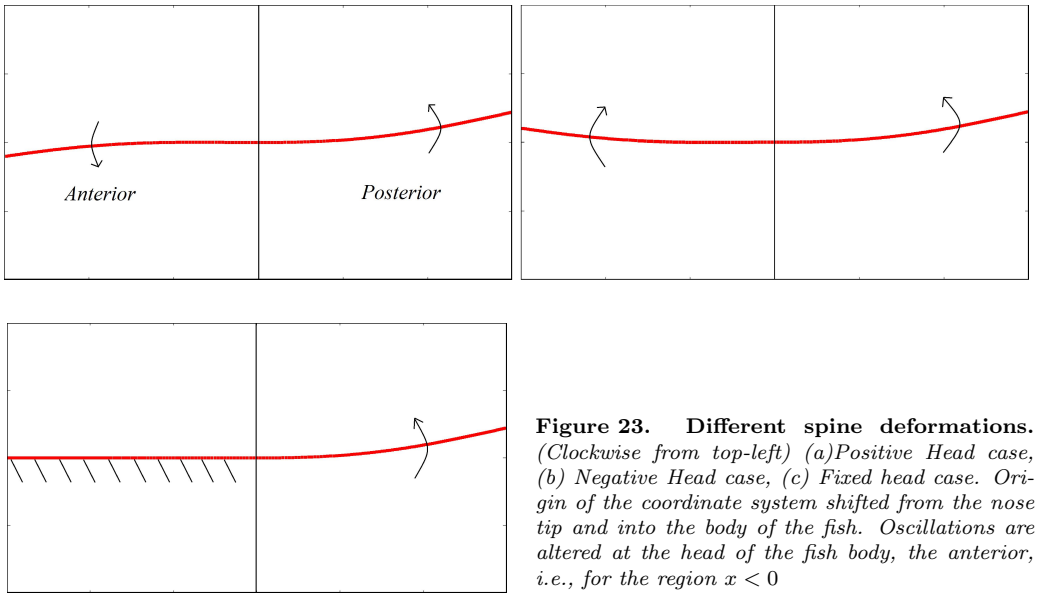

Figure 23. Different spine deformations. *(Clockwise from top-left) (a)Positive Head case, (b) Negative Head case, (c) Fixed head case. Origin of the coordinate system shifted from the nose tip and into the body of the fish. Oscillations are altered at the head of the fish body, the anterior, i.e., for the region $x < 0$*

The fish given a tail tip amplitude of 0.3 which provided with a highly unstable swim due to vortex interactions, which we wish to improve. The three cases above with a value of $\delta = 0.25$ were compared with the base case with no altered spine deformation, i.e., δ=0. A graphically representation of varying velocity is given in Figure 24.

As it can be observed, the altered spine deformations led to serious improvements in the motion of the fish. All three cases managed to significantly stabilize the swim. However, as we can see, the most significant improvement is obtained by utilizing the negative head type of spine deformations. This method led to a much stable swim motion and provided the largest value for average horizontal speed. An investigation of flow structures showcased lack of influential vortex structures accumulating at nose and breaking off to

affect swim motion. This would explain the smooth motion and almost periodic velocity plots. The positive head case provides for the largest value of maximum velocity attained but an erratic trend for velocity plots, and results for fixed head case were in between the other two cases. The evaluation of the flow solutions confirmed the presence of large vortex structures in these cases, which formed and detached at the nose, travelling along the fish body and adding propulsion through interactions at random time instances, creating velocity spikes. Since we are concerned about the overall optimization of fish swim, we pick the negative case for further studies.

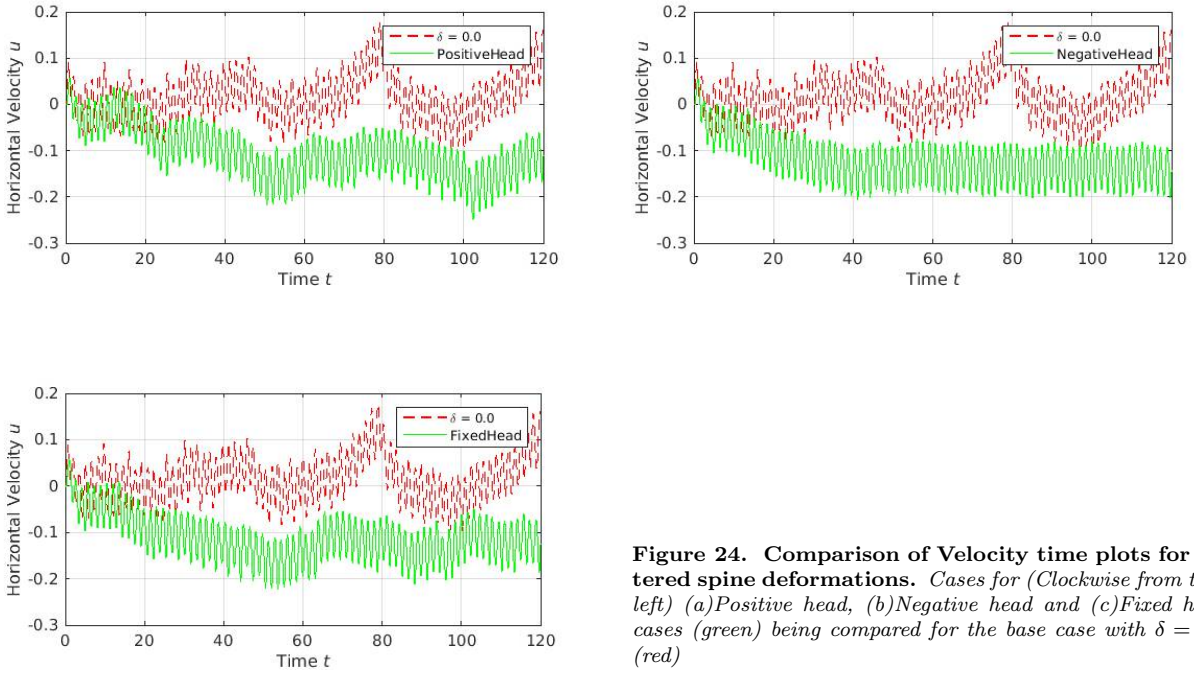

Figure 24. Comparison of Velocity time plots for altered spine deformations. *Cases for (Clockwise from top-left) (a)Positive head, (b)Negative head and (c)Fixed head cases (green) being compared for the base case with* $\delta = 0.0$ *(red)*

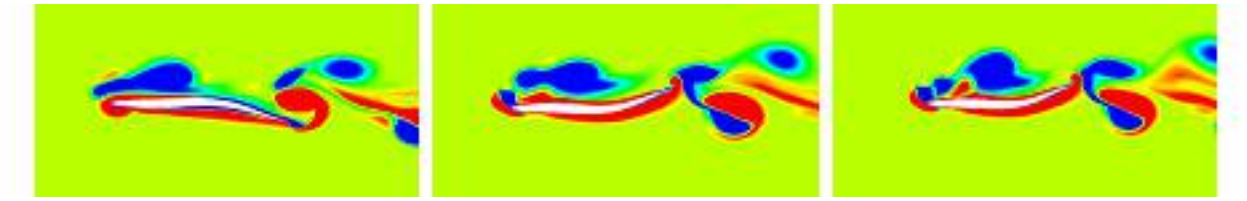

Figure 25. Vorticity plots for Positive Head case. *Plots at time t = 87.9, 92.6, 95.8 sec respectively showing the presence of large vortex structures being formed and accumulated on the upper body surface that detach, travel down the body, interacting with it and creating random fluctuations in velocity, as shown in velocity time plots. Positive head case was unable to effectively/sufficiently destroy these structures.*

Figure 26. Vorticity plots for Negative Head case. *Plots at time t = 87.9, 92.6, 95.8 sec respectively showing the effective destruction of large vortex structures, that are being formed and try to accumulate at the anterior, into smaller structures that detach and do not affect the motion of the fish significantly, resulting no random fluctuations in velocity, as shown in velocity time plots.*

The mode of vortex interaction for above cases appear to correspond to Slaloming.[28] The wake consists of a pair of vortices, one produced by the tail and the other consisting of travelled anterior vortices, which can be more clearly observed on top-right of Figure 26. This, however, may only be due to the fish generating a velocity in the vertical direction. It is also worth noticing that the body postures for negative head case are extremely similar to the hemispherical ones observed in dead trouts experiencing thrust when towed in the wake of a cylinder, shown in Figure 27. Similar body postures would enable efficient travel of anterior vortices (comparable to cylinder vortices) along the fish body without accumulation, resulting in a stabilized swim.

Figure 27. Dead Trout Kàrmàn gait kinematics.[28]

C. Variation of δ

We seek out to investigate the effects of the position of our origin on the spine for the sinusoidal spine deformations. This is achieved by varying δ on the spine coordinate. Previously, we investigated the case for $\delta = 0.25$ whereby we obtained optimized swim for the negative head case. The propuslion was investigated for value of $\delta = 0.1, 0.2, 0.3, 0.4$. Velocity plots are shown in Figure 28.

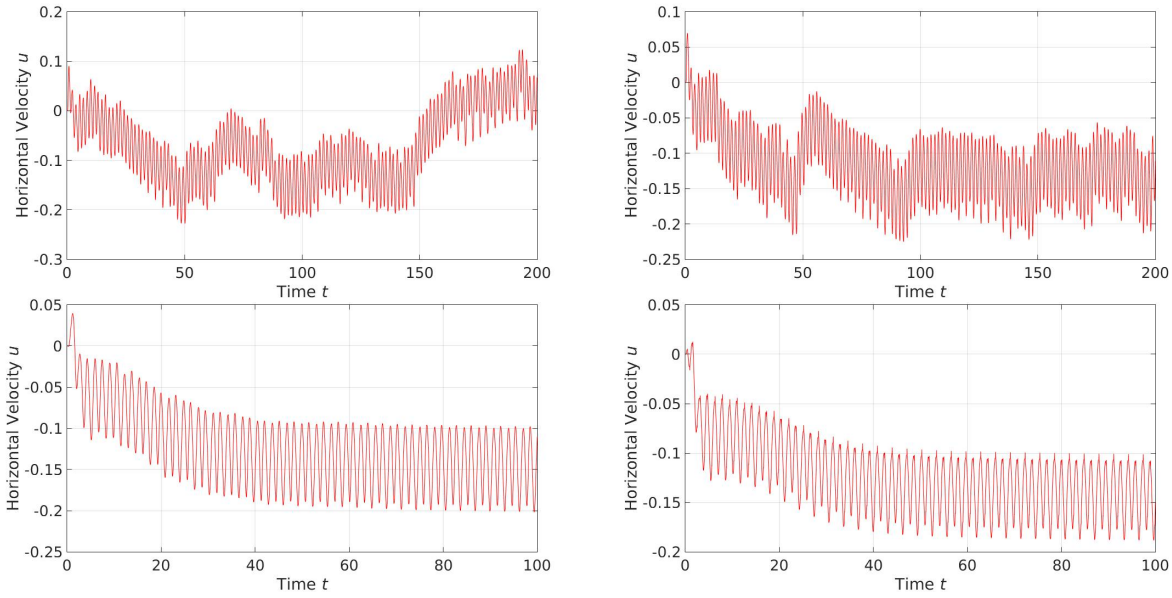

Figure 28. *Velocity time plots for different values of δ. Top to bottom, left to right : δ = 0.1, 0.2, 0.3, 0.4*

As the point of zero spine deformation was made to travel further into the fish body, the fish swim stabilized. This can be observed for the cases for: $\delta = 0.1$ wherein the swim is erratic and sudden, random changes in velocity manage to change/alternate the direction of motion of the swim (attributed to destructive vortices); $\delta = 0.2$ wherein the swim is stabilized to obtain a constant forward motion of swim, yet there exists presence of random spikes in horizontal swim velocities; $\delta = 0.3$ provided for the most stable case with the velocity profile periodic after initial acceleration, and presence of no random spikes in velocity magnitudes or erratic changes in direction of motion. A study of flow solutions confirmed the lack of large vortex structures that where responsible for the unstable and erratic swim present in previous two cases and the base case with

$\delta = 0.0$. Further increases in δ reduces the magnitude of maximum horizontal velocity achieved, relating of decrease in propulsion efficiencies/power.

D. Frequency of fish head/anterior deformation

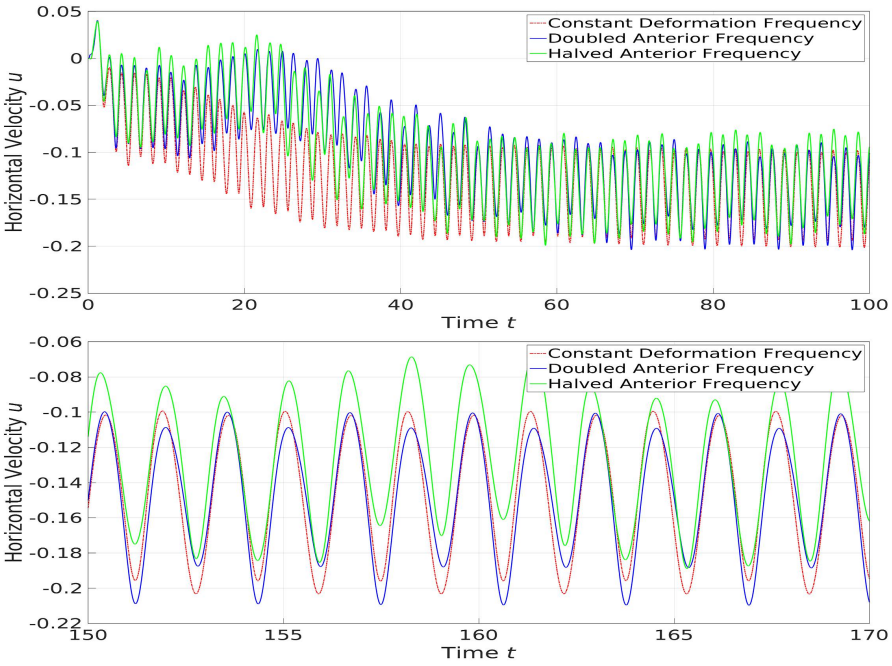

Figure 29. Variation of frequency of spine deformations at anterior. *Velocity time plots for faster anterior deformations ($f = 4$) represented in blue and slower anterior deformations ($f=1$) represented in green, compared with the case for equal frequencies for both anterior and posterior. Frequency of posterior deformations remains constant at $f=2$ for all cases.*

Placing our coordinate origin at δ from the nose tip, for simplicity, we define the anterior of the fish by $x < 0$ and the posterior by $x > 0$. The effects of different frequencies of oscillations for the anterior and posterior regions of the spine was investigated with an intention to observe effects on the disruption of the vortex formations and accumulations at the tip of the fish nose. The anterior was made to deform slower or faster with respect to the posterior. This was compared with the base case for equal frequencies of oscillations for both regions, shown in Figure 29.

Faster head deformations were seen to provide the fish with higher horizontal velocity magnitudes. Slower head deformations results in slower swim speeds and slightly erratic swims, with fluctuations associated with vortex interactions. Faster anterior deformations would result in more effective destruction of vortex structures generated at the nose and improved propagation of these smaller vortices along the body and towards the tail without accumulation near the nose, since it is dependent on the interactions between the nose deformations during their formation. On the contrary, the opposite effects were noticed for slower anterior deformations, with the accumulation of structures being faster than their breakup through interaction with nose deformations. Both cases, however, result in decreased initial accelerations from rest, i.e., the fish takes more time to proceed towards its steady value of average horizontal velocity.

The results obtained are comparable to Liao's[24] experimental observations of trouts selectively activating their anterior muscles during Kàrmàn gait to exploit their energies. Comparing their cylinder vortices to vortices generated at the anterior, to efficiently destroy/utilize these structures and ensure their travel along the body without accumulation, changes need to made to anterior spine deformations, which is what our study focused on. This helps us optimize body kinematics ensuring stable swim with high propulsive efficiencies.

E. Improvement of higher amplitude swims

Using the results and optimized values obtained by these case studies for tail tip amplitude of 0.3, we can apply them to improve the swim for higher tail tip amplitudes which previously provided us with a

motion in the backward direction. This is shown in Figure 30 for the case of $A = 0.4$, wherein the case for $\delta = 0.0$, provided us with a backward swim shown in the plot as a positive average horizontal velocity. Applying $\delta = 0.3$, the negative head movement helped provide the fish with a forward swim with a negative average horizontal velocity. However, the swim can further be optimized as we observe the presence of vortex structures that cause sudden changes in velocity profiles. Higher amplitudes of spine deformations, have been shown to create more persistent and larger vortex structures at the anterior. This asserts that different swim conditions require different sets of optimized spine deformation/shape parameters to effectively get rid of anterior vortex accumulations so as to stabilize the swim.

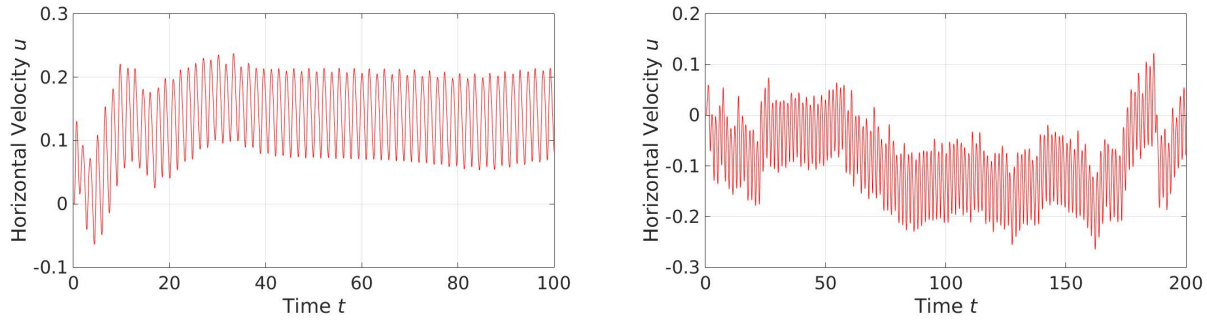

Figure 30. *(Left) Higher amplitude A=0.4 and δ=0.0; (Right) Optimized values for A=0.3 of δ=0.3 and negative head case applied for A=0.4*

An attempt for achieving further improvements to the above was made by observing the effects of providing the different amplitudes of oscillations to the anterior half, with respect to the posterior. Since the vortex structures obtained for $A = 0.4$ were larger, we try to ascertain whether a multiplied magnitude of anterior deformation could lead to more effective eliminations of vortex formations and accumulations at the nose. Two cases where studied, one having a doubled and the other having halved anterior deformations with respect to the improved case obtained above.

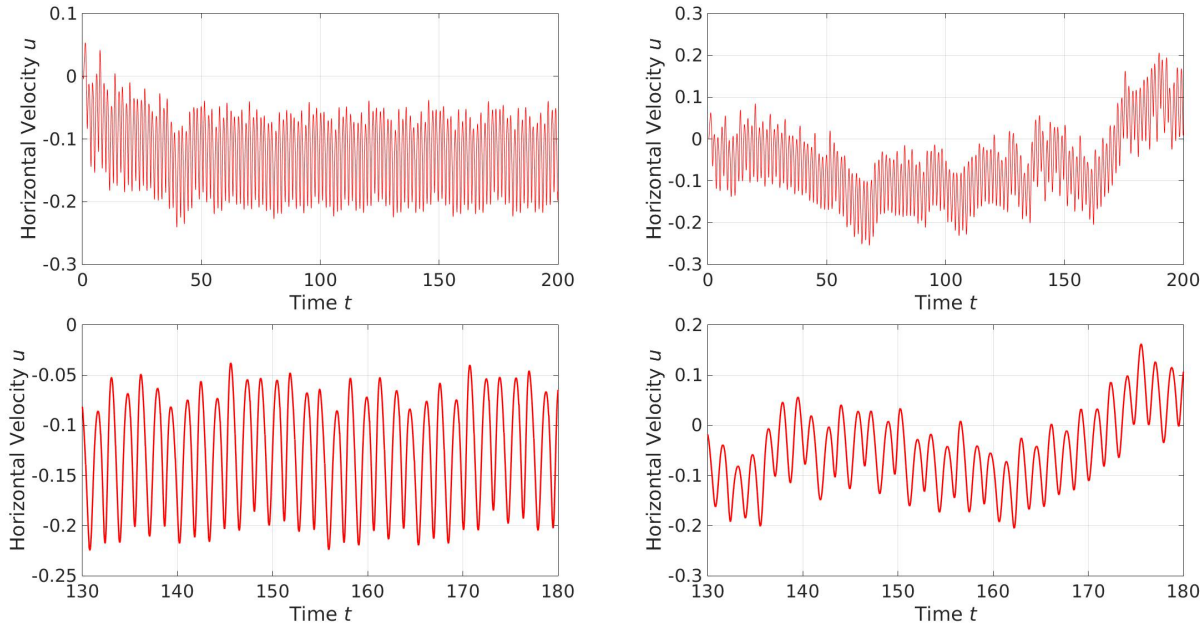

Figure 31. *Velocity time plots for varied amplitude of deformations of anterior. Doubled(right) and Halved(left)*

The velocity plots shown in Figure 31 validate our expectations that a multiplied amplitude of anterior deformations would result in better destruction of vortices and thus a swim with improved stability. As we can observe, the velocity profiles were made almost periodic. The opposite can be observed for the halved case, where random initial fluctuations in swim velocity creates a total change in direction of motion of the fish (Destructive vortex interactions).

The above solutions are consistent with Liao's[24] hypothesis and experimental observations wherein vortices defined Kàrmàn gait kinematics. Different fish-spine deformations would result in vortex structures having different sizes, strength, etc. Hence, the most efficient deformations of anterior regions of the body would change to adapt to these structures. This can also be confirmed with providing doubled anterior amplitude of deformation to the previous case of $A = 0.3$, wherein no improvements in swim were observed. Swims with higher amplitudes generate larger anterior vortices and thus, would require different optimized body deformations to ensure swim stability.

VI. Conclusions

In this study, thunniform fish motions were investigated numerically, with a particular focus on the interactions between the vortex structures generated by the anterior part of the fish body with the body and with the tail vortex wake. Significant interactions were observed at time instances in which sharp changes in the magnitude of otherwise steady, periodically oscillating horizontal velocity are noticeable. As expected, these sudden changes were found to result from the fish extracting rotational energy from the vortices which augmented the forward motion of the fish. The fish was able to increase its propulsive thrust, and could thus accelerate with a sharp rise in velocity magnitudes. The results obtained are consistent with the experimental visualizations and numerical studies on foil propulsion and vorticity control conducted in the literature.

Further, another scenario was investigated wherein the forward motion of the fish was significantly disrupted by destructive interactions with these vortex structures. These vortices were strong enough to change the direction of motion. Their persistence near the tail during stall and initial backward motion, and increase in size due to tail oscillations enabled the fish to attain large backward velocities. The velocity of motion of the fish, however, showed large variations since the backward motion is mostly sustained by these vortices and the fish tail continued to experience reduced, but considerable pressure-related propulsive forces in the forward direction.

Knowing the dependence of fish motion on the vortex interactions and tail wake structures, we proceeded towards altering spine deformations and shapes to create significant increases in swim stability, propulsive efficiencies and power, for different conditions. By focusing on varying the nature of anterior spine deformations, improved swim stability was achieved for motions with high tail-tip amplitudes. These modifications on anterior spine deformations resulted in the destruction of large anterior vortices into smaller structures and their efficient travel along the fish body. This provided a stable extraction of energy from the smaller structures during the entirety of the fish motion in contrast to sudden interactions at random instances of time, which can be opposed to forward motion of the fish. The modified deformations appear to be comparable to observed body kinematics of fishes extracting incoming vortex energy during Kàrmàn gait whilst selectively activating only their anterior muscles. This showcases the importance of anterior body postures during the presence of influential vortex structures. There is thus a need to modify the deformations to attain optimized head angles, ensuring reduced generation/influence of erratic vortices breaking off at the anterior and, thus, highly stable swims.

References

[1]Lauder, G. V. and Madden, P. G. A., "Learning from Fish: Kinematics and Experimental Hydrodynamics for Roboticists," *International Journal of Automation and Computing*, Vol. 4, 2006, pp. 325–335.

[2]Drucker, E. G. and Lauder, G. V., "Experimental Hydrodynamics of Fish Locomotion: Functional Insights from Wake Visualization," *Integrative and Comparative Biology*, Vol. 42, 2002, pp. 243–257.

[3]Flammang, B. E., Alben, S., Madden, P. G., , and Lauder, G. V., "Functional Morphology of the Fin Rays of Teleost Fishes," *Journal of Morphology*, Vol. 274, 2013, pp. 1044–1059.

[4]Tytell, E. D. and Lauder, G. V., "The Hydrodynamics of Eel Swimming I. Wake Structure," *Journal of Experimental Biology*, Vol. 207, 2004, pp. 1825–1841.

[5]Lauder, G. V., "Function of the Caudal Fin during Locomotion in Fishes: Kinematics, Flow Visualization, and Evolutionary Patterns," *Americal Zoologist*, Vol. 40, 2000, pp. 101–122.

[6]Drucker, E. G. and Lauder., G. V., "Function of Pectoral Fins in Rainbow Trout: Behavioral Repertoire and Hydrodynamic Forces," *Journal of Experimental Biology*, Vol. 206, 2003, pp. 813–826.

[7]Bergmann, M. and Iollo, A., "Modeling and simulation of fish-like swimming," *Journal of Computational Physics*, Vol. 230, 2011, pp. 329–348.

[8]Melli, J. B., *A hierarchy of models for the control of fish-like locomotion*, Ph.D. thesis, Department of Mechanical and Aerospace Engineering, Princeton University, 2008.

[9]Galls, S. F. and Rediniotis, O. K., "Computational simulation of the autonomous navigation of a biomimetic underwater vehicle," *, AIAA Journal*, April.

[10]Barrett, D., Triantafyllou, M., Yue, D., Grosenbaugh, M., and Wolfgang, M., "Drag reduction in fish-like locomotion," *Journal of Fluid Mechanics*, Vol. 392, 2000, pp. 183–212.

[11]Wolfgang, M., Anderson, J., Grosenbaugh, M., Yue, D., and Triantafyllou, M., "Near-body flow dynamics in swimming fish," *Journal of Experimental Biology*, Vol. 202, 1999, pp. 2303–2327.

[12]Cheng, J. and Chahine, G., "Computational hydrodynamics of animal swimming: boundary element method and three-dimensional vortex wake structure," *Comparative Biochemistry and Physiology*, Vol. 131, 2001, pp. 51–60.

[13]Webb, P., "Form and function in fish swimming," Scientific american inc., 1984.

[14]Sfakiotakis, M., Lane, D. D., Davies, J., and C., B., "Review of Fish Swimming Modes for Aquatic Locomotion," *Journal of Oceanic Engineering*, Vol. 24, 1999, pp. 237–252.

[15]Müller, U. K., den Heuvel, B. L. E. V., Stamhuis, E. J., and Videler, J. J., "Fish foot prints: Morphology and energetics of the wake behind continuously swimming mullet (Chelon Labrosus Risso)," *Journal of Experimental Biology*, Vol. 200, 1997, pp. 28932906.

[16]Rosen, M. W., "Water flow about a swimming fish," Tech. rep., US Naval Ordnance Test Station TP 2298, China Lake, CA, 1959.

[17]Gemmell, B. J., Colin, S. P., Costello, J. H., and Dabiri, J. O., "Suction-based propulsion as a basis for efficient animal swimming," *Nature Communications*, Vol. 6, 2015, pp. 1–8.

[18]Liao, J. C., Beal, D. N., Lauder, G. V., and Triantafyllou, M. S., "Fish exploiting vortices decrease muscle activity," Science, 302, 2003.

[19]Liao, J. C., Beal, D. N., Lauder, G. V., and Triantafyllou, M. S., "The Kàrmàn gait: novel body kinematics of rainbow trout swimming in a vortex street," *Journal of Experimental Biology*, Vol. 206, 2003, pp. 1059–1073.

[20]Fausch, K. D., "Experimental Analysis of Microhabitat Selection by Juvenile Steelhead (Oncorhynchus mykiss) and Coho Salmon (O. kisutch) in a British Columbia Stream," *Canadian Journal of Fisheries and Aquatic Sciences*, Vol. 50, 1993, pp. 1198–1207.

[21]Gerstner, C. L., "Use of substratum ripples for flow refuging by Atlantic cod (Gadus morhua)," Environmental biology of fishes, 1998.

[22]Gopalkrishnan, R., Triantafyllou, M., Triantafyllou, G., and Barrett, D., "Active vorticity control in a shear flow using a flapping foil," *Journal of Fluid Mechanics*, Vol. 274, 1994, pp. 1–21.

[23]Streitlien, K., Triantafyllou, G. S., and Triantafyllou, M. S., "Efficient foil propulsion through vortex control," *AIAA Journal*, Vol. 34, No. 11, 1996, pp. 2315–2319.

[24]Liao, J. C., "Neuromuscular control of trout swimming in a vortex street: implications for energy economy during the Kàrmàn gait," *Journal of Experimental Biology*, Vol. 207, 2004, pp. 3495–3506.

[25]Gray, J., "Studies in animal locomotion. VI. The propulsive powers of the dolphin," *Journal of Experimental Biology*, Vol. 13, 1936, pp. 192–199.

[26]Anderson, J. M., *Vorticity control for efficient propulsion*, Ph.D. thesis, Massachusetts Institute Technology/Woods Hole Oceanographic Institute Joint Program, Woods Hole, MA.

[27]Barrett, D. S., *Propulsive efficiency of a flexible hull underwater vehicle*, Ph.D. thesis, Massachusetts Institute Technology, Cambridge.

[28]Beal, D. N., Hover, F. S., Triantafyllou, M. S., Liao, J. C., and Lauder, G. V., "Passive propulsion in vortex wakes," *Journal of Fluid Mechanics*, Vol. 549, 2006, pp. 385–402.

[29]Webb, P., "Body form, locomotion and foraging in aquatic vertebrates," *Americal Zoologist*, Vol. 24, 1984, pp. 107–120.

[30]Lakshminarayan, V. K., *Computational Investigation of Micro-Scale Coaxial Rotor Aerodynamics in Hover*, Ph.D. thesis, Department of Aerospace Engineering, University of Maryland, College Park.

[31]Duraisamy, K. and Baeder, J. D., "High resolution wake capturing methodology for hovering rotors," *Journal of the American Helicopter Society*, Vol. 52, No. 2, 2007, pp. 110–122.

[32]Duraisamy, K., McCroskey, W. J., and Baeder, J. D., "Analysis of wind tunnel wall interference effects on subsonic unsteady airfoil flows," *Journal of aircraft*, Vol. 44, No. 5, 2007, pp. 1683–1690.

[33]Aranake, A. C., Lakshminarayan, V. K., and Duraisamy, K., "Computational analysis of shrouded wind turbine configurations using a 3-dimensional RANS solver," *Renewable Energy*, Vol. 75, 2015, pp. 818–832.

[34]Bremseth, J. and Duraisamy, K., "Computational analysis of vertical axis wind turbine arrays," *Theoretical and Computational Fluid Dynamics*, 2016, pp. 1–15.